On the potential for RF heating in MRI to affect metabolic rates and ^{18}FDG signal in PET/MR: simulations of long-duration, maximum normal mode heating

Giuseppe Carluccio,[a] Yu-Shin Ding, Jean Logan, and Christopher M. Collins
Department of Radiology, New York University, New York, NY 10016, USA

(Received 26 April 2016; revised 6 November 2016; accepted for publication 14 November 2016; published 30 January 2017)

Purpose: To examine the possibility that MR-induced RF power deposition (SAR) and the resulting effects on temperature-dependent metabolic rates or perfusion rates might affect observed 18FDG signal in PET/MR.
Methods: Using numerical simulations of the SAR, consequent temperature increase, effect on rates of metabolism or perfusion, and [18FDG] throughout the body, we simulated the potential effect of maximum-allowable whole-body SAR for the entire duration of an hour-long PET/MR scan on observed PET signal for two different 18FDG injection times: one hour before onset of imaging and concurrent with the beginning of imaging. This was all repeated three times with the head, the heart, and the abdomen (kidneys) at the center of the RF coil.
Results: Qualitatively, little effect of MR-induced heating is observed on simulated PET images. Maximum relative increases in PET signal (26% and 31% increase, respectively, for the uptake models based on metabolism and the perfusion) occur in regions of low baseline metabolic rate (also associated with low perfusion and, thus, greater potential temperature increase due to high local SAR), such that PET signal in these areas remains comparatively low. Maximum relative increases in regions of high metabolic rate (and also high perfusion: heart, thyroid, brain, etc.) are affected mostly by the relatively small increase in core body temperature and thus are not affected greatly (10% maximum increase).
Conclusions: Even for worst-case heating, little effect of MR-induced heating is expected on 18FDG PET images during PET/MR for many clinically relevant applications. For quantitative, dynamic MR/PET studies requiring high SAR for extended periods, it is hoped that methods like those introduced here can help account for such potential effects in design of a given study, including selection of reference locations that should not experience notable increase in temperature. [https://doi.org/10.1002/mp.12046]

Key words: metabolism, MRPET, perfusion, SAR, simulations, temperature

1. INTRODUCTION

The advantages of simultaneously acquiring the complimentary information available in MRI and PET have led to a growth in the number of systems and applications for PET/MR.[1–8] MRI provides anatomical information with high temporal and spatial resolution as well as a variety of other physiologic information without the need for ionizing radiation. Using a wide range of radiopharmaceuticals, PET can rapidly locate regions of abnormal function with high specificity. Despite concerns regarding challenges to acquiring patient-specific attenuation maps with PET/MR as opposed to PET/CT,[9] early comparisons indicate performance of PET/MR to compare very well to PET/CT,[3–5] with PET/MR being preferable in some studies,[6–8] Potential advantages of PET/MR include good soft tissue contrast, accurate reconstruction of PET images with use of real-time motion tracking in MRI,[10] and significant reduction in patient exposure to ionizing radiation.

Effects of temperature on PET images have been observed on animals.[11,12] Given the potential for the radiofrequency energy used in MRI to cause heating of tissues[13,14] and the expectation for temperature-dependent metabolic rates[15,16] and perfusion rates,[15,17] here we consider the possibility for the RF heating in MRI to affect the observed signal in 18FDG PET during PET/MR in human tissues. This is done using numerical simulations considering the RF power deposition (SAR) and temperature distributions, metabolic rates or perfusion rates, and consequent timecourse of 18FDG throughout the body for two different 18FDG injection times with respect to initiation of an hour-long PET/MR scan with maximum allowable SAR during the entire scan.

In this work, we present our methods and examine cases where the subject is exposed to high SAR for a long time. While we conclude that for the vast majority of routine clinical exams there should be no significant effect of MR heating on PET signal, we believe the methods we present here may also be useful to researchers with more specialized interests (especially those attempting dynamic, quantitative PET with high-SAR MR sequences) who may need to ensure unintended consequences of their study design will not potentially affect their observations.

2. MATERIALS AND METHOD

First, simulations of temperature increase throughout the human body due to MR-related RF heating were performed for three different scenarios. Specifically, the electromagnetic fields were simulated for a body-size 16-element, 60 cm diameter, high-pass birdcage coil having legs 40 cm long and 5 cm wide, and operating at 128 MHz (corresponding to the operating frequency of 3T MRI systems) with a model of the human body positioned at three different locations, as if to image the head, the heart, and the kidneys (Fig. 1). The electromagnetic simulations were performed with commercial software xFDTD (Remcom, State College, PA) and a human body model based on a manual segmentation of the National Library of Medicine's "Visible Male" data set, having a meshgrid resolution 5 mm × 5 mm × 5 mm.[18] The entire model contained 891507 voxels. The simulated electromagnetic fields were then normalized so that the head-average Specific energy Absorption Rate (SAR; a measure of heating) was 3.2 W/kg for the simulation with the head positioned in the center of the coil, and the whole-body average SAR was 2 W/kg for the other two cases. These are the maximum values recommended under the IEC guidelines for normal mode operation of MRI systems.[14]

In each of the three configurations, temperature (T) for an application of these maximum allowable SAR values continuously for 60 min was estimated with the Pennes' bioheat equation[19]

$$\rho c \frac{\partial T}{\partial t} = \nabla \cdot (k \nabla T) - W_{\rho_{bl} c_{bl}} (T - T_{bl}) + Q + \rho SAR \quad (1)$$

where c is the heat capacity, ρ the material density, k is the thermal conductivity, W is a parameter related to blood perfusion rate, Q is the heat generated by metabolism, and the subscript bl indicates values for blood, and SAR, the heat source due to RF absorption, is given by the formula

$$SAR = \frac{\sigma |E|^2}{\rho} \quad (2)$$

where σ and E represent, respectively, electrical conductivity and the electric field.

The temperature simulation was performed with an in-house finite difference code[20] which also allowed for heat loss to the surrounding air and was shown previously to give accurate results, including at the boundaries.[20] Additionally, a variety of parameters in addition to local temperature T were updated at each iteration. Specifically, the blood temperature parameter T_{bl}, corresponding also to the core body temperature, is allowed to increase through time according to the total energy absorbed by the body through the MRI scan according to a previously described model which also considers respiration and additional heat loss mechanisms,[21] and both the local metabolic rate Q and the local blood perfusion W are allowed to change according to the local temperature T.[15,17]

A variety of physiological models for accumulation of 18FDG by tissue containing multiple compartments within local tissue in addition to a component for blood concentration are used to fit measured concentrations of 18FDG through time. In order to predict 18FDG as a function of temperature through time, use of a model with more than one component in tissue would require a priori knowledge of the concentrations and exchange rates of FDG associated with the various compartments in all tissues through the body at rest, as well as their dependence on temperature. As such information for all tissues in the body is not now available in the literature, we considered two different models, each with only one compartment in tissue: one where uptake of 18FDG is dominated by metabolism, and one where it is dominated by perfusion. In both cases, it is assumed that all 18FDG taken up by the tissue would remain there to maximize the potential effects of temperature.

The often-cited Maxwell-Boltzmann dependence between metabolic rate Q, the average activation energy E, and temperature T.[16]

$$Q \propto e^{-\frac{E}{kT}} \quad (3)$$

for human body temperatures can be approximated well as[15,17]

$$Q = Q_0 (1.1)^{T - T_0} \quad (4)$$

In this work, Q was varied with temperature according to Eq. (4), and in the metabolism-based model perfusion was held at the baseline levels throughout the imaging period to maximize the increase in temperature and thus the effects of MR-related heating on PET signal.

For the perfusion-based model, local blood perfusion rate W was varied as a function of local temperature according to the relationship

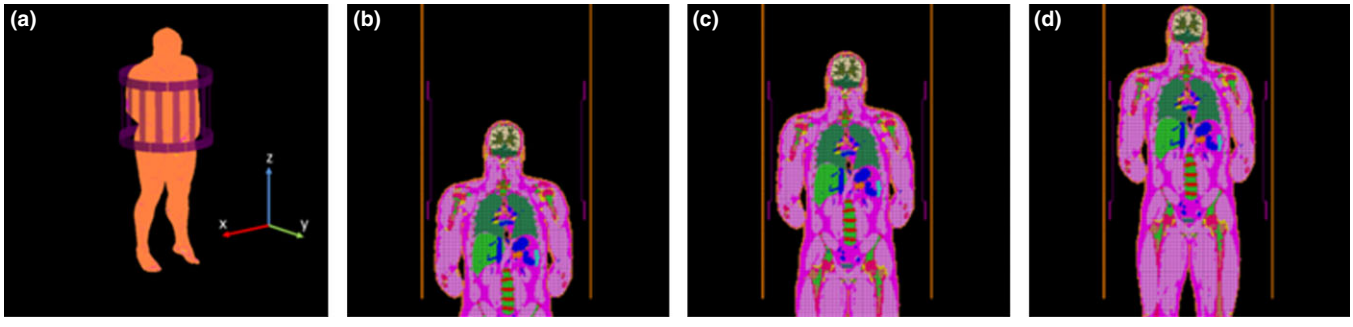

FIG. 1. Schematic of the geometry of the problem with a whole-body model in a birdcage coil at 128 MHz (a), and of the three different positions of the body in the coil: as for imaging the head (b), the heart (c), and the kidney (d). [Color figure can be viewed at wileyonlinelibrary.com]

$$W = \begin{cases} W_0 & T \leq 39°\mathrm{C} \\ W_0(1 + S_B(T - 39)) & 39°\mathrm{C} < T < 44°\mathrm{C} \\ W_0 5 S_B & T \geq 44°\mathrm{C} \end{cases} \quad (5)$$

where T_0, Q_0 and W_0 represent, respectively, the temperature, the metabolic rate, and the perfusion at the equilibrium temperature (with no SAR applied), and S_B is a coefficient set to $0.8°C^{-1}$.[15,17] The values of the material density ρ, the heat capacity c, the heat conductivity k, of Q_0 and W_0 used in the simulations for different tissues were gathered from an online database.[22] For the perfusion-based model, metabolic rate was allowed to increase with temperature in order to maximize the effect of MR-related heating on temperature and PET signal.

The relative concentrations of FDG through time and space were calculated using two simple two-compartment model describing the FDG concentration in the blood ($[FDG]_{blood}$), and the local concentration in the tissues ($[FDG]_{tissue}$), where in one case the concentration in the tissues depends on perfusion W, and in the other it depends on the metabolic rate Q.

For the case where uptake is based on perfusion, the concentrations are estimated with the following differential equations:

$$\begin{cases} \frac{\partial}{\partial t}[FDG]_{blood} = -\lambda[FDG]_{blood} + \delta(t - t_i) \\ \frac{\partial}{\partial t}[FDG]_{tissue} = -\lambda[FDG]_{tissue} + W[FDG]_{blood} \end{cases} \quad (6)$$

while in case the uptake is based on metabolic rate, they are estimated with:

$$\begin{cases} \frac{\partial}{\partial t}[FDG]_{blood} = -\lambda[FDG]_{blood} + \delta(t - t_i) \\ \frac{\partial}{\partial t}[FDG]_{tissue} = -\lambda[FDG]_{tissue} + Q[FDG]_{blood} \end{cases} \quad (7)$$

where the he decay constant λ is equal to

$$\frac{\lambda = \ln(2)}{t_{1/2}} \quad (8)$$

and $t_{1/2}$ is the half-life of FDG, estimated to be 110 min[23] and the delta function δ indicates a sudden increase in $[FDG]_{blood}$ at the time of injection, t_i. Although the terms W and Q in Eq. (6) and (7) do not have the same units of λ, Eq. (6) and (7) express the proportionality between the concentration of the tracer in the tissue and either the local perfusion or the local metabolism. For this reason, all the PET signals images obtained with the solution of the equations have been normalized as described later. Equation (6) and (7) have been solved numerically where at each iteration the values of Q and W have been updated depending on the local temperature value.

For each of the three positions of the coil, two different timecourses were considered with respect to the time of FDG injection relative to the onset of a one-hour period of MR/PET imaging including MR-related heating at the maximum allowable levels. In one case the imaging period began immediately after the injection of the FDG agent, which is sometimes used in dynamic quantitative analysis, and in the other the imaging period began one hour after the injection, which is typical in clinical exams. The accumulated PET signal through time

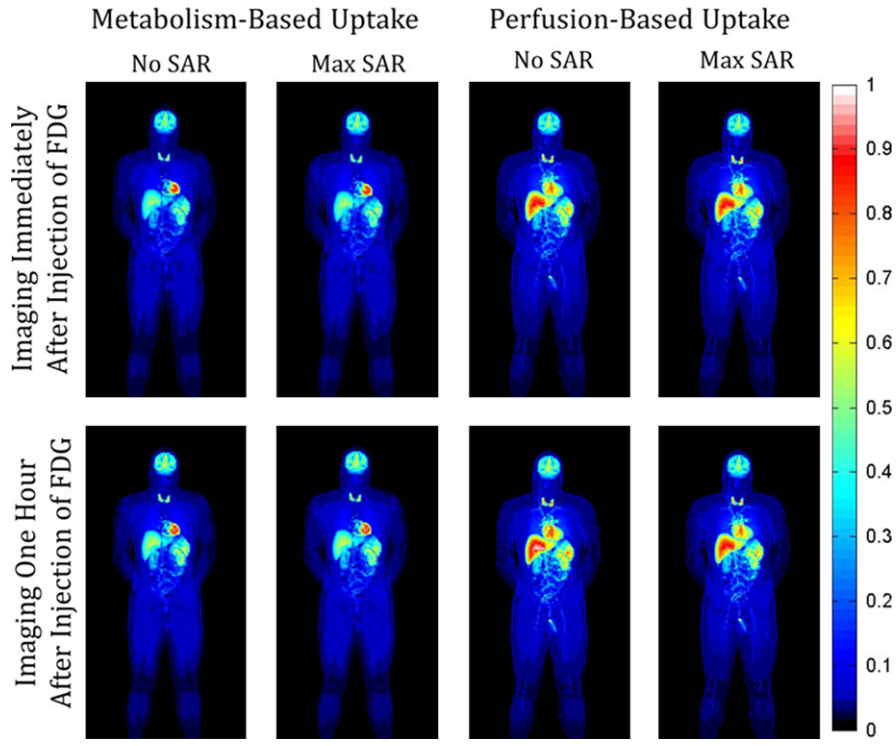

FIG. 2. Accumulated PET signal through time for both the uptake models based on metabolism and the perfusion, for the RF coil centered around the heart, plot of the signal intensity just after and one hour after the injection of the FDG contrast, in case the SAR is absorbed, and in case no heat is applied. The images have been normalized to the maximum value found in each timecourse. [Color figure can be viewed at wileyonlinelibrary.com]

was calculated as the integral of the local $[FDG]_{tissue}$ through the entire 60 min imaging time as projected in the anterior-posterior direction. For comparison, in all three imaging scenarios and both timecourses, the PET signal was also calculated for zero SAR, such that $T = T_0$ and $Q = Q_0$ throughout time and space. Again, in the metabolism-based model (the model in Eq. (7)), perfusion is kept constant and equal to W_0 (not temperature dependent as in Eq. (5)) to simulate maximal temperature increase.

Standardized Uptake Value (SUV) was estimated by normalizing the concentration of 18FDG at the end of the imaging period (when temperatures are highest) to produce a value of 8 in the heart, which is in the range of the expected values for a healthy subject.[24]

3. RESULTS

Figure 2 shows the accumulated PET signal through time for the case when the body is positioned with the heart near the center of the RF coil, both in the case of maximum allowable SAR and no SAR applied throughout the imaging period, and for both the metabolism-based and perfusion-based models. Figure 3 shows both the temperature distributions and the percentage increase in the signal intensity with maximum allowable SAR.

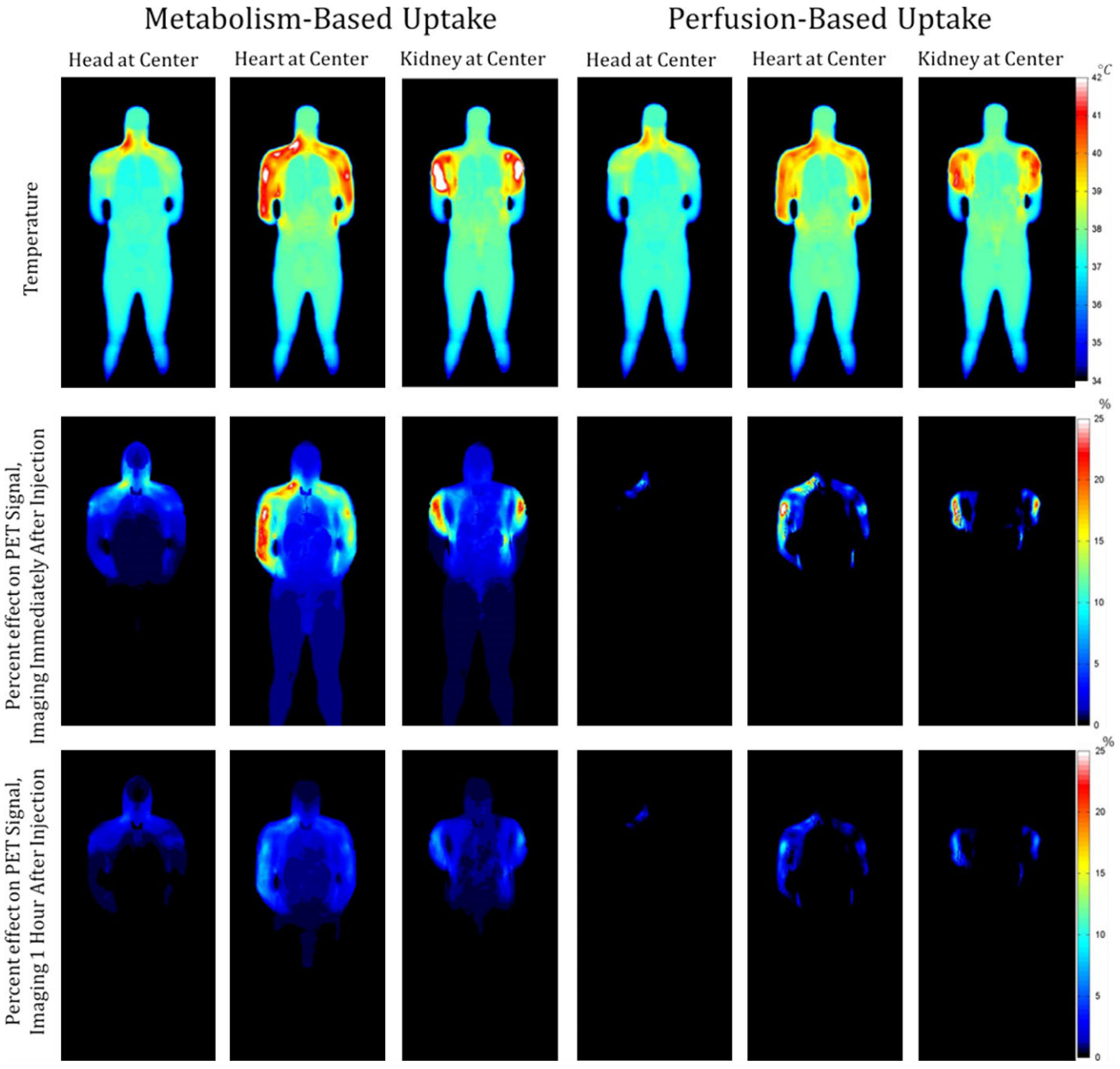

FIG. 3. For both uptake models and all imaging positions of the MRI coil, temperature distribution on a coronal slice through the body at the end of the imaging period (top row), and increase in the accumulated PET signal relative to that when no SAR is applied. [Color figure can be viewed at wileyonlinelibrary.com]

TABLE I. Maximum temperatures, maximum percentage metabolic rate, and perfusion increases at the end of the examination for the perfusion uptake model.

	Imaging the head	Imaging the heart	Imaging the kidneys	Region of occurrence
Max T	40.5 °C	41.8 °C	43.0 °C	Skeletal muscle
Max T increase	3.95 °C	6.09 °C	6 °C	Skeletal muscle
Max % increase in Q	45.8%	77.6%	77.2%	Skeletal muscle
Max % effect on PET signal imaging, starting at injection	10.68%	31.35%	28.45%	Skeletal muscle
Max % effect on PET signal, imaging starting 1hr post-injection	3.41%	10.01%	9.08%	Skeletal muscle
Max increase in Q	2.45 W/kg (2.8%)	4.9 W/kg (5.6%)	3.63 W/kg (4.2%)	Thyroid
Max core Temperature	37.12 °C	37.40 °C	37.40 °C	
Max % increase in W	127.04%	229.39%	233.29%	
Max increase in W	$4.95\frac{ml}{kg\times min}$	$8.06\frac{ml}{kg\times min}$	$41.07\frac{ml}{kg\times min}$	

TABLE II. Maximum temperatures and maximum percentage metabolic rate increases at the end of the examination for the metabolic rate uptake model.

	Imaging the head	Imaging the heart	Imaging the kidneys	Region of occurrence
Max T	42.23 °C	44.78 °C	44.81 °C	Skeletal muscle
Max T increase	5.52 °C	7.90 °C	7.57 °C	Skeletal muscle
Max % increase in Q	69.19%	112.21%	105.7%	Skeletal muscle
Max % effect on PET signal imaging, starting at injection	16.38%	25.96%	21.5%	Skeletal muscle
Max % effect on PET signal, imaging starting 1hr post-injection	5.23%	8.29%	6.8%	Thyroid
Max increase in Q	2.55 W/kg (2.8%)	5.14 W/kg (5.6%)	5.48 W/kg (42.48%)	Thyroid
Max core Temperature	37.12 °C	37.40 °C	37.40 °C	

The maximum values of local temperature, local temperature increase, core body temperature, percent increase in the metabolic rate, absolute increase in metabolic rate, percent increase in perfusion, absolute increase in perfusion and percent increase in the PET signal intensity are presented in Table I and II. Since the initial concentration of FDG in tissues is set to 0, smaller variations in percent increase are observed when the imaging occurs one hour after the injection, because much of the uptake in tissues then occurs while there is no heating. The maximum temperature during MR-induced heating (first row), maximum temperature increase due to MR-induced heating (second row), maximum percent effect on metabolic rate, Q (third row), maximum percent effect on PET signal intensity imaging immediately after FDG injection (fourth row), and maximum percent effect on PET signal intensity imaging one hour after FDG injection (fifth row) all occur in the skeletal muscle of the shoulders or arms in all cases (with the head, heart, and kidney at the center of the coil), except for the maximum increase in Q when the coil is centered on the kidneys and perfusion is not allowed to change according to temperature, whence occurs in a focal region of the colon. The last two rows of Table I report also the maximum absolute and relative increase in perfusion. Because muscle tissue has a low baseline perfusion rate (37 mL/min/kg) its temperature is much more readily affected by SAR than tissue with a much higher perfusion rate, and because it has a low baseline metabolic rate (0.9 W/kg) even a large relative increases in perfusion and metabolic rate still result in low perfusion, metabolic rates, FDG uptake, and PET signal Fig. 4 compared with tissues having high baseline perfusion and metabolic rates such as heart, brain, and thyroid. Except for the case where maximum increase in Q occurs in the colon, the maximum absolute increases in metabolic rate (sixth row) occurred in the thyroid, which has the highest baseline metabolic rate (87.1 W/kg). The percent increase in metabolic rate at these locations, however, was relatively low (2.8%, 5.6%, and 4.2%, when imaging the head, heart, and kidneys, respectively, and perfusion is allowed to change according to temperature increase). Due to the high rate of perfusion of the thyroid (5624 mL/min/kg), the temperature there closely followed the core body temperature (last row), which increased by only 0.12, 0.4, and 0.4 °C when imaging the head, heart, and kidneys respectively. The maximum signal intensity values of the simulated PET Fig. 2 are located in the area of the heart due to a combination of its size and its high perfusion and metabolic rates. Even in these extreme cases simulated PET images are not significantly affected by the increase in the perfusion and metabolic rate (Fig. 2), enough that the change might be clinically relevant. For example, Fig. 5 shows that for both the uptake models the maximum SUV value reached in muscle is well below the range of SUV values expected in malignant muscle tumors.[25] Also, for the case where the maximum increase in metabolic rate occurs in the colon, the estimated SUV is equal to 3.2

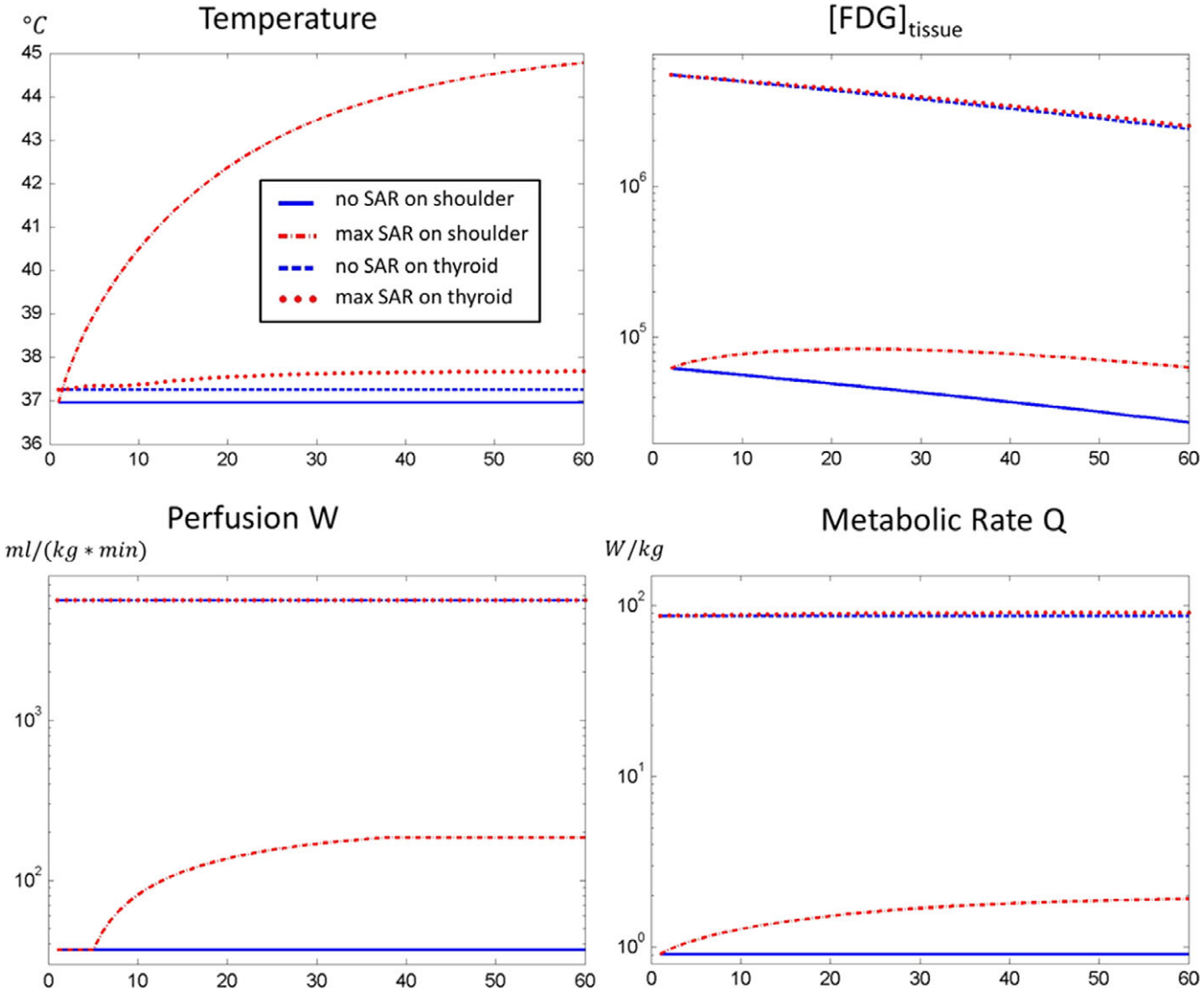

FIG. 4. Plots of Temperature, concentration of FDG, perfusion, and metabolic rate when imaging the heart begins at the time of injection for two locations: skeletal muscle at the location of greatest temperature increase and the thyroid. A blue continuous line and a blue dashed line are used to indicate the change in the parameters in the muscle and the thyroid, respectively, when no SAR is applied. A dotted line and a sequence of dashes and dots are used for the muscle and the thyroid locations, respectively, when high SAR is applied. All the plots refer to the metabolism-based model except the plots of the perfusion variation, which are obtained from the perfusion-based model. [Color figure can be viewed at wileyonlinelibrary.com]

while a recommended threshold SUV for diagnosing colon cancer is closer to 5.[26]

4. DISCUSSION

We have simulated the potential effects of MR-related heating on PET signal involving continual SAR levels at the maximum allowable levels under normal mode operation continuously for one hour. In clinical practice today it is unusual to go above normal mode operating limits, and also unusual to exceed exam times of 20 to 30 min. Because clinical exams typically require considerably less time than one hour and because SAR levels during an actual exam will typically not be at or above the maximum allowable levels for longer than a few minutes we have considered extreme cases, and in practice any effects on PET signal should be significantly lower than those seen here. Even in these extreme cases simulated PET images are not significantly affected by the increase in the metabolic rate due to the MRI exam, because the most significant changes of the accumulated PET signal (around 30%) occur in tissues such as muscles having low values of perfusion and metabolic rate. Hence, even in this worst-case heating scenario the observed differences are not likely to affect most clinical studies, where (for example) locations with a fundamentally high level of activity, such as high metabolic rates in malignant tumors for FDG-based studies, are sought,[27,28] and where higher SUV is expected. Regions of high metabolic rates also typically are highly perfused, such that their temperature is more closely tied to the core body temperature and less affected by local sources of

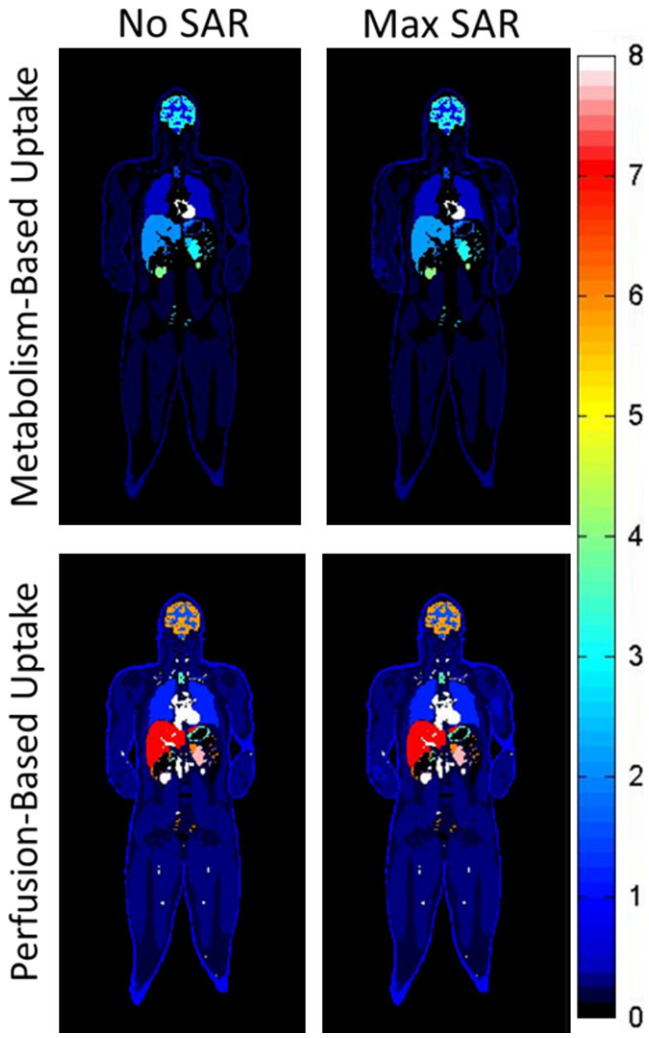

FIG. 5. Estimated SUV on a single coronal slice for both the uptake models based on metabolism and perfusion for the RF coil centered around the heart with imaging beginning at the time of injection and in the case when no heat is applied. [Color figure can be viewed at wileyonlinelibrary.com]

heat. This does not rule out the possibility, however, that – depending on the tissue of interest and the intended accuracy of measurement – quantitative, dynamic PET studies[26] might be affected by high SAR levels applied for an extended period of time: for example, if uptake in skeletal were used as reference for the other tissues in a quantitative dynamic exam, a significant change there it may affect the other measurements. It is hoped that in such cases, methods like those used here could help ensure study design such that no unanticipated effects of MR-related heating would affect the PET signal by design of MR sequences with lower SAR or selection of reference locations that are not expected to be affected by MR-related heating.

ACKNOWLEDGMENTS

We are grateful to Linda Moy, MD, for her insightful suggestions related to clinically relevant SUV thresholds and the potential to select regions of low-SAR for reference in quantitative, dynamic exams, and to the NIH for funding through R01 EB011551 and P41 EB017183.

CONFLICTS OF INTEREST

The authors have no relevant conflicts of interest to disclose.

[a]Author to whom correspondence should be addressed. Electronic mail: giuseppe.carluccio@nyumc.org.

REFERENCES

1. Parikh N, Friedman KP, Shah SN, Chandarana H. Practical guide for implementing hybrid PET/MR clinical service: lessons learned from our experience. *Abdom Imaging*. 2015;40:1366–1373.
2. Schlemmer HP, Pichler BJ, Schmand M et al. Simultaneous MR/PET imaging of the human brain: feasibility study. *Radiology*. 2008;248:1028–1035.
3. Schwenzer NF, Schraml C, Muller M et al. Pulmonary lesion assessment: comparison of whole-body hybrid MR/PET and PET/CT imaging-pilot study. *Radiology*. 2012;264:551–558.
4. Drzezga A, Souvatzoglou M, Eiber M et al. First clinical experience with integrated whole-body PET/MR: comparison to PET/CT in patients with oncologic diagnoses. *J Nucl Med*. 2012;53:845–855.
5. Chandarana H, Heacock L, Rakheja R et al. Pulmonary nodules in patients with primary malignancy: comparison of hybrid PET/MR and PET/CT imaging. *Radiology*. 2013;268:874–881.
6. Brendle CB, Schmidt H, Fleischer S, Braeuning UH, Pfannenberg CA, Schwenzer NF. Simultaneously acquired MR/PET images compared with sequential MR/PET and PET/CT: alignment quality. *Radiology*. 2013;268:190–199.
7. Schafer JF, Gatidis S, Schmidt H et al. Simultaneous whole-body PET/MR imaging in comparison to PET/CT in pediatric oncology: initial results. *Radiology*. 2014;273:220–231.
8. Catalano OA, Rosen BR, Sahani DV et al. Clinical impact of PET/MR imaging in patients with cancer undergoing same-day PET/CT: initial experience in 134 patients–a hypothesis-generating exploratory study. *Radiology*. 2013;269:857–869.
9. Hofmann M, Pichler B, Scholkopf B, Beyer T. Towards quantitative PET/MRI: a review of MR-based attenuation correction techniques. *Eur J Nucl Med Mol I*. 2009;36:93–104.
10. Furst S, Grimm R, Hong I et al. Motion correction strategies for integrated PET/MR. *J Nucl Med*. 2015;56:261–269.
11. Hildebrandt IJ, Su H, Weber WA. Anesthesia and other considerations for in vivo imaging of small animals. *ILAR J*. 2008;49:17–26.
12. Fueger BJ, Czernin J, Hildebrandt I et al. Impact of animal handling on the results of 18F-FDG PET studies in mice. *J Nucl Med*. 2006;47:999–1006.
13. Yarmolenko PS, Moon EJ, Landon C et al. Thresholds for thermal damage to normal tissues: an update. *Int J Hyperthermia*. 2011;27:320–343.
14. International Electrotechnical Commission. International standard, medical equipment – part 2: particular requirements for the safety of magnetic resonance equipment for medical diagnosis. 3rd revision. 2010.
15. Bernardi P, Cavagnero M, Pisa S, Piuzzi E. Specific absorption rate and temperature elevation in a subject exposed in the far-field of radio-frequency sources operating in the 10-900 MHz range. *IEEE T Biomed Eng*. 2003;50:295–303.
16. Gillooly JF, Brown JH, West GB, Savage VM, Charnov EL. Effects of size and temperature on metabolic rate. *Science*. 2001;293:2248–2251.
17. Wang Z, Lin JC, Vaughan JT, Collins CM. Consideration of physiological response in numerical models of temperature during MRI of the human head. *J Magn Reson Imag*. 2008;28:1303–1308.
18. Collins CM, Smith MB. Calculations of B-1 distribution, SNR, and SAR for a surface coil adjacent to an anatomically-accurate human body model. *Magn Reson Med*. 2001;45:692–699.

19. Pennes HH. Analysis of tissue and arterial blood temperatures in the resting human forearm. *J Appl Physiol*. 1948;1:93–122.
20. Collins CM, Liu W, Wang JH et al. Temperature and SAR calculations for a human head within volume and surface coils at 64 and 300 MHz. *J Magn Reson Imag*. 2004;19:650–656.
21. Adair ER, Berglund LG. On the thermoregulatory consequences of NMR imaging. *Magn Reson Imaging*. 1986;4:321–333.
22. IT'IS Foundation. Tissue Property Database. http://www.itis.ethz.ch/virtual-population/tissue-properties/overview.
23. Oberg K, Eriksson B. Nuclear medicine in the detection, staging and treatment of gastrointestinal carcinoid tumours. *Best Pract Res Clin Endocrinol Metab*. 2005;19:265–276.
24. Heuscha P, Buchbendera C, Beiderwellenb K et al. Standardized uptake values for [18F] FDG in normal organ tissues: comparison of whole-body PET/CT and PET/MRI. *Eur J Radiol*. 2013;82:870–876.
25. Shin DS, Shon OJ, Han DS, Choi JH, Chun KA, Cho IH. The clinical effi cacy of 18F-FDG-PET/CT in benign and malignant musculoskeletal tumors. *Ann Nucl Med*. 2008;22:603–609.
26. Strauss LG, Koczan D, Klippel S et al. Dynamic PET with (18)F-Deoxyglucose (FDG) and quantitative assessment with a two-tissue compartment model reflect the activity of glucose transporters and hexokinases in patients with colorectal tumors. *Am J Nucl Med Mol Imaging*. 2013;3:417–424.
27. Avril N, Bense S, Ziegler SI et al. Breast imaging with fluorine-18-FDG PET: quantitative image analysis. *J Nucl Med*. 1997;38:1186–1191.
28. Yonekura Y, Benua RS, Brill AB et al. Increased accumulation of 2-deoxy-2-[18F]Fluoro-D-glucose in liver metastases from colon carcinoma. *J Nucl Med*. 1982;23:1133–1137.